The Astrophysical Journal, 798:19 (9pp), 2015 January 1 doi:10.1088/0004-637X/798/1/19


# SMALL-SCALE STRUCTURING OF ELLERMAN BOMBS AT THE SOLAR LIMB

C. J. Nelson[1,2], E. M. Scullion[3,4], J. G. Doyle[1], N. Freij[2], and R. Erdélyi[2]
[1] Armagh Observatory, College Hill, Armagh BT61 9DG, UK
[2] Solar Physics and Space Plasma Research Centre, University of Sheffield, Hicks Building, Hounsfield Road, Sheffield S3 7RH, UK
[3] Institute of Theoretical Astrophysics, University of Oslo, NO-0371 Oslo, Norway
[4] Astrophysics Research Group, School of Physics, SNIAM, Trinity College Dublin, Dublin 2, Ireland
*Received 2014 January 30; accepted 2014 October 20; published 2014 December 15*

## ABSTRACT

Ellerman bombs (EBs) have been widely studied in recent years due to their dynamic, explosive nature and apparent links to the underlying photospheric magnetic field implying that they may be formed by magnetic reconnection in the photosphere. Despite a plethora of researches discussing the morphologies of EBs, there has been a limited investigation of how these events appear at the limb, specifically, whether they manifest as vertical extensions away from the disk. In this article, we make use of high-resolution, high-cadence observations of an Active Region at the solar limb, collected by the CRisp Imaging SpectroPolarimeter (CRISP) instrument, to identify EBs and infer their physical properties. The upper atmosphere is also probed using the *Solar Dynamic Observatory*'s Atmospheric Imaging Assembly (*SDO*/AIA). We analyze 22 EB events evident within these data, finding that 20 appear to follow a parabolic path away from the solar surface at an average speed of 9 km $s^{-1}$, extending away from their source by 580 km, before retreating back at a similar speed. These results show strong evidence of vertical motions associated with EBs, possibly explaining the dynamical "flaring" (changing in area and intensity) observed in on-disk events. Two in-depth case studies are also presented that highlight the unique dynamical nature of EBs within the lower solar atmosphere. The viewing angle of these observations allows for a direct linkage between these EBs and other small-scale events in the H$\alpha$ line wings, including a potential flux emergence scenario. The findings presented here suggest that EBs could have a wider-reaching influence on the solar atmosphere than previously thought, as we reveal a direct linkage between EBs and an emerging small-scale loop, and other near-by small-scale explosive events. However, as previous research found, these extensions do not appear to impact upon the H$\alpha$ line core, and are not observed by the *SDO*/AIA EUV filters.

*Key words:* Sun: chromosphere – Sun: magnetic fields – Sun: photosphere

## 1. INTRODUCTION

The solar atmosphere is a complex and dynamic environment, filled with a myriad of structures, ranging from large-scale coronal loops and prominences to small-scale granules and photospheric magnetic bright points (MBPs). With the increased resolution and coverage of both ground-based and space-borne instrumentation in recent years, it has become possible to observe and analyze a wider range of solar phenomena in greater detail. As certain ground-based instruments, such as the CRisp Imaging SpectroPolarimeter (CRISP; see Scharmer 2006; Scharmer et al. 2008), are capable of resolving the lower solar atmosphere on spatial scales close to 90 km, a wide variety of small-scale events have been discussed, specifically in terms of how they interact with the wider environment.

Ellerman bombs (often shortened to EBs within the literature) are one example of small-scale events observed in the lower solar atmosphere. Widely identified as brightenings inferred from 0.5–5 Å into the wings of the H$\alpha$ line profile, EBs often form co-spatially with regions of strong magnetic field, specifically in mixed polarity regions (see, for example, Pariat et al. 2004; Vissers et al. 2013). First observed by Ellerman (1917), these small-scale events are reported to have diameters ranging from around 300 km to 750 km and lifetimes often less than 20 minutes (as estimated by, e.g., Zachariadis et al. 1987; Watanabe et al. 2011; Nelson et al. 2013a), meaning they are observed at the lower limits of current instrumentational capabilities.

Recently, Nelson et al. (2013a) presented an analysis, using a thresholding technique, of small-scale regions of intense brightening in the H$\alpha$ line wings that were inferred using the Interferometric BIdimensional Spectrometer (IBIS; Cavallini 2006), situated at the Dunn Solar Telescope (DST), and found a dynamic behavior within many events. It was concluded that many of these small events may be EBs and that higher-resolution data should decrease the average observed size of EBs. However, as was discussed by Rutten et al. (2013), the strong network observable within the H$\alpha$ wings may also influence the thresholding technique, meaning that a proportion of the less dynamic small events could be purely network brightenings and are more likely associated with MBPs.

Due to both the dynamic nature of EBs and their co-spatial formation with strong magnetic fields, it is widely hypothesized that these events are observational evidence of magnetic reconnection in the upper photosphere. Georgoulis et al. (2002) presented an analysis of data collected during the Flare Genesis Experiment (see Murphy 1996), inferring three cartoon topologies that could lead to magnetic reconnection within the lower solar atmosphere. Two of these correspond to the formation of $\Omega$ and $\cup$ shaped topologies due to flows within the lower atmosphere, thought to be consistent with small bi-polar regions observed in magnetogram data. By applying a linear force-free extrapolation pioneered by Demoulin et al. (1997), Pariat et al. (2004, 2007) discussed the nature of the photospheric magnetic fields close to EB events. It was found that approximately 87% of EBs formed co-spatially with

∪-shaped magnetic topologies and, hence, concluded that a serpentine flux emergence model could lead to EB formation. Furthermore, Matsumoto et al. (2008) presented observations of flows co-spatial to EBs potentially supporting the magnetic reconnection model. It was found that down- and up-flows in the photosphere and chromosphere existed, respectively, suggesting bi-dimensional plasma ejection by an explosive event, possibly sourced in the upper photosphere. Interestingly, during a detailed analysis of three suspected EBs by Bello González et al. (2013), one event was observed to penetrate through the chromospheric canopy into the H$\alpha$ line core, indicating that large vertical flows within these events can sometimes occur.

A small number of studies exist that discuss observations of EBs located close to the limb of the Sun. Roy & Leparskas (1973) presented observations of EBs for two distinct Active Regions (ARs), one close to the disk center and one toward the limb. It was found that the apparent lifetime of EBs was shorter when observed at the limb and, importantly, that vertical extensions were evident. This work was expanded upon by Kurokawa et al. (1982), who analyzed a large group of sunspots at the limb. These observations confirmed vertical extensions of EBs and provided the first quantification of lengths, at approximately 800 km, and widths, below 450 km for 80% of EBs. It is interesting to note, that this estimate of width agrees well with the measured diameters of EBs on the disk by, for example, Georgoulis et al. (2002) and Nelson et al. (2013a). More recently, using high-resolution H$\alpha$ data, Watanabe et al. (2011) discussed the small-scale dynamics of EBs at a viewing angle of $\mu = 0.67$, finding evidence of rapid increases in area, intensity, and vertical extensions. These "flaring," morphological changes were identified as evidence of a high-energy driver within the lower atmosphere, specifically, magnetic reconnection. It is clear that further analysis of events observed close to the limb at high inclination angles, as presented here, could provide interesting and useful results about the physical nature of EBs.

As well as observations, numerical methods have also been exploited to analyze the physical properties of EBs. Fang et al. (2006) presented a semi-empirical model, finding that increased temperature in the lower atmosphere could lead to H$\alpha$ line profiles with increased intensity in the line wings, analogous to EBs. Numerical simulations, using the Coordinate Astronomical Numerical Softwares (CANS) code, were presented in two- and three-dimensions by Isobe et al. (2007) and Archontis & Hood (2009), respectively, who found that flux emergence from below the photosphere could lead to ∪-shaped magnetic topologies and associated brightening events. More recently, a study was conducted by Nelson et al. (2013b) who found H$\alpha$ wing brightenings, analogous to EBs, co-spatial with magnetic reconnection events within a MPS/University of Chicago Radiative MHD (MURaM) simulation box. This reconnection occurred in the upper photosphere and led to increased temperatures, which explained the enhanced H$\alpha$ wings, as hypothesized by Fang et al. (2006). Flows were also found, analogous to those observed by Matsumoto et al. (2008), around the reconnection site. Interestingly, both the observations and the simulations showed Fe I 6302.5 Å line core brightenings, which have been widely associated with magnetic reconnection (see, for example, Shelyag et al. 2007).

In this article, we analyze both the morphology of EBs observed at the limb and any potential relationship between these events and the surrounding plasma. We structure our work as follows. In Section 2, we discuss the data analyzed in this article; Section 3 presents our results, including a statistical analysis of EBs within these data and two individual case-studies. We discuss the implications of our findings in Section 4.

## 2. OBSERVATIONS

The ground-based data analyzed in this research were collected using the CRISP instrument attached to the Swedish 1 m Solar Telescope (SST; Scharmer et al. 2003) during a period of good seeing on 2012 June 21. A large field-of-view (FOV), situated around AR 11506 ($xc = 893''$, $yc = -250''$ with respect to the disk center), containing three sunspots was selected for observations during the period from 7:15:09 UT until 7:48:25 UT. $\alpha$ line scans, sampling 35 evenly spaced spectral positions (each with eight repetitions) between −2 Å and +1.2 Å from the line core (6562.8 Å) were obtained, and further processed using the Multi-Object Multi-Frame Blind Deconvolution (MOMFBD; van Noort et al. 2005) image restoration method. We followed the standard procedures in the reduction pipeline for CRISP data (Rodriguez et al. 2014), which includes the post-MOMFBD correction for differential stretching suggested by Henriques (2012; also see Sekse et al. 2012 for more details). Following this reduction (which included dark- and flat-fielding), the pixel size of these data was 0.″059, which corresponds to approximately 43 km in a transverse scale (future distance measurements within this article will discuss distances measured using this transverse scale), and the temporal cadence was approximately 7.7 s, hence allowing for a detailed analysis of EB events. To conduct the analysis presented here, we exploit the excellent widget-based CRISPEX package (see Vissers & Rouppe van der Voort 2012).

We also make use of data taken by the *Solar Dynamics Observatory*'s Atmospheric Imaging Assembly (*SDO*/AIA; see Lemen et al. 2012) instrument. These data image the entire solar disk within the UV spectrum using filters around 1600 Å and 1700 Å. These data have effective spatial and temporal resolutions of around 1000 km and 48 s, respectively. The outer layer of the solar atmosphere is also observed using a number of EUV filters; however, in the analysis presented here, we show only the 304 Å filter. Each EUV image has a spatial resolution of approximately 1000 km and a temporal resolution of 24 s.

In Figure 1, we present an overview of the FOV analyzed within this article. Clockwise from the top left image, we plot the array returned by the narrow-band CRISP filter for each of −1.8 Å, −0.95 Å, +0.95 Å, and 0 Å at approximately 7:36:20 UT. Within this FOV, sit three sunspots (two in the southern part of the FOV and one in the northern section) as well as a large plage region. It is around these sunspots that all EBs occur that are of interest for this analysis. What is immediately apparent from these images, is that the underlying photosphere is obscured by absorption resulting from the chromospheric material in the H$\alpha$ line core in the bottom left image. The complex fibril structures observed in the line core appear to be present higher in the atmosphere, hence, potentially obscuring some of the vertical extent of the EBs in this data set. We overlay three boxes on all images highlighting the three EBs analyzed in detail.

## 3. RESULTS

### 3.1. EB Statistics

Within the H$\alpha$ line profile, EBs are easily identified as increases in intensity observed in images around 0.5 Å either

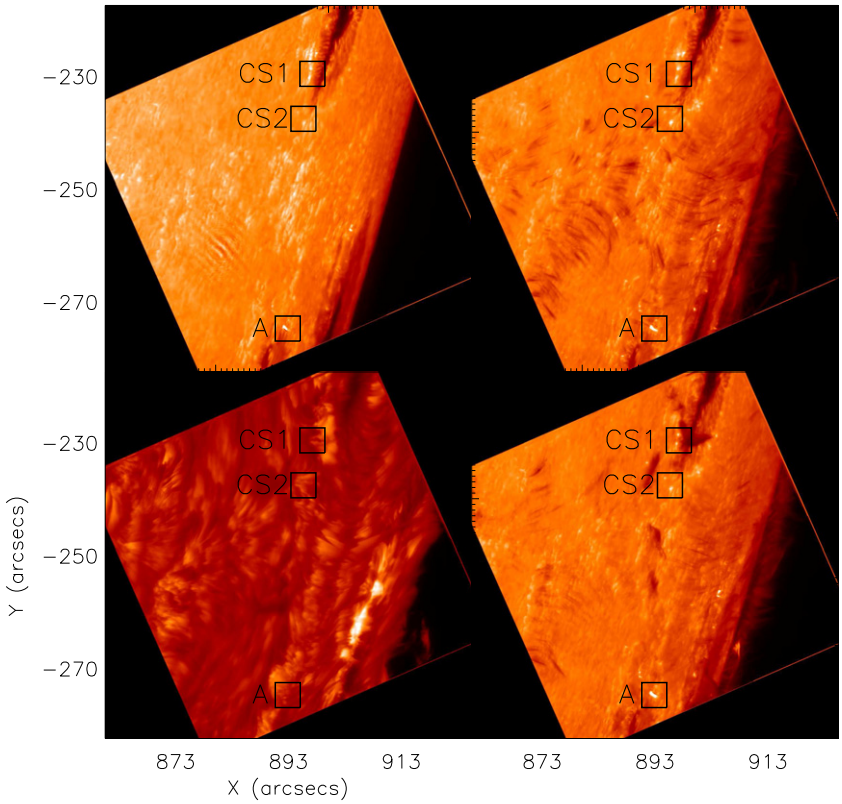


**Figure 1.** FOV of AR 11506 analyzed within this article (corrected for local instrumental wavelength shifts), sampled at four positions within the H$\alpha$ line scan: the far blue wing (approximately −1.8 Å; top left), the near blue wing (−0.95 Å; top right), the H$\alpha$ line core (0 Å; bottom left), and the red wing (+0.95 Å; bottom right). The black boxes in each image indicate the regions of interest analyzed in the following sections. A known artifact of the image reconstruction process is visible in the far blue wing at (883, −260).

side of the line core. Modern imaging-spectrometers, such as the CRISP instrument, are able to provide fast wavelength tuning between each line position included in a line scan allowing confident identification of EBs. Here, we define EBs as events which show both intensity increases which are greater than 1.5 times the intensity of the nearby quiet Sun in the wings of the H$\alpha$ line profile and also a dynamic, explosive nature evidenced by imaging data. Fragmenting EBs observed within these data are classified as being a single event. If an event dies completely and does not recur for five frames, any new co-spatial brightening is classified as a new EB event. By employing these guidelines, we remove the influence of network bright points such as those situated at $xc = 893''$, $yc = -250''$, which have a consistently lower line wing intensity throughout these observations, as compared with EB wing intensity excess. Overall, we confidently identify 22 EB events within these observations. Three regions which contain EBs during these observations are highlighted in Figure 1 by black boxes for further analysis.

In Figure 2, we plot normalized line profiles for two of the representative EB events highlighted in Figure 1 (solid lines; scaled to the maximum intensity of the EB profile). The significant intensity increases within these events are evident when compared to the local quiet Sun (dotted lines; also scaled to the maximum intensity of the EB profile). To highlight the percentage increase in intensity, we also plot the inverted (for visual ease) difference between the quiet Sun and the EB events (dashed lines). The difference between line-wing intensities peaks at over −0.5 indicating a doubling of the intensity from the quiet Sun for these EB events in their respective frames. Such gradients between EBs and the background atmosphere are not observed in every frame as the intensity of individual events appears to vary on timescales of seconds (as was discussed by Qiu et al. 2000). We note that an acceptable thresholding value is highly dependent on a number of factors such as the instrumentation, data processing techniques, and the seeing at the time of the observations.

After the identification of all apparent EBs in the data, each event was carefully analyzed to determine its lifetime and area. As the definitions between EBs and the background are strong in these data (as is shown in Figure 2), the estimation of the lifetime was easily completed by analyzing the evolution of each EB through time. The initial and final frames of each event were identified visually by studying the imaging data which show the evolution of these events clearly. Overall, the average lifetime of EBs in these data was found to be approximately seven minutes, comparable to previous researches by, e.g., Roy & Leparskas (1973), Watanabe et al. (2011), and Nelson et al. (2013a). The shortest and longest-lived events, respectively, were three minute and around 20 minutes. The distribution of lifetimes within these data is plotted in Figure 3 (left).

We plot both the peak width and peak length of each EB event against lifetime in Figures 3 (center) and (right). It is apparent (although not significantly correlated) that longer lived EBs appear to be larger (as previously discussed by Roy & Leparskas 1973). As the majority of EBs exhibit parabolic morphological evolutions through time (as evidenced in Figure 4), it appears that the strength of the initial driver is a key variable in defining

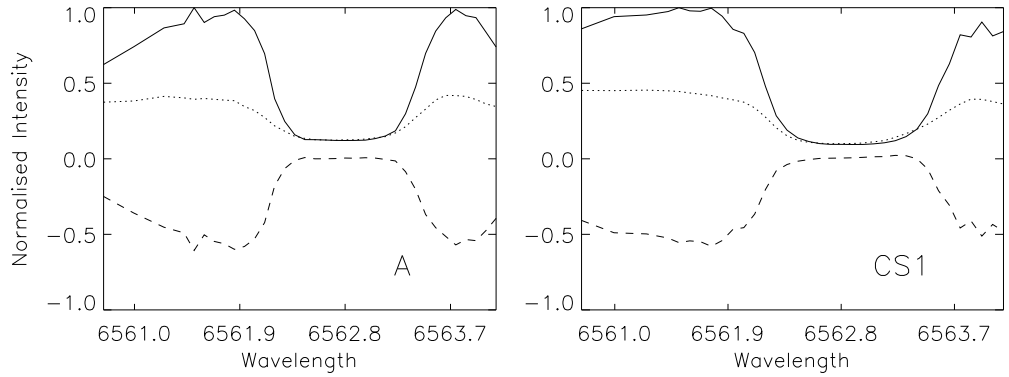


**Figure 2.** Normalized line profiles of two representative EBs compared to the background intensity of the nearby quiet Sun. The EB line profiles (solid lines) for (left) box "A" and (right) box "CS1" in Figure 1 compared to the quiet Sun (dotted line). The dashed line shows the inverted (for clarity) difference in normalized intensity between the quiet Sun and EB profiles. The heightened line wings of the EB line profile are representative of other events within these data.

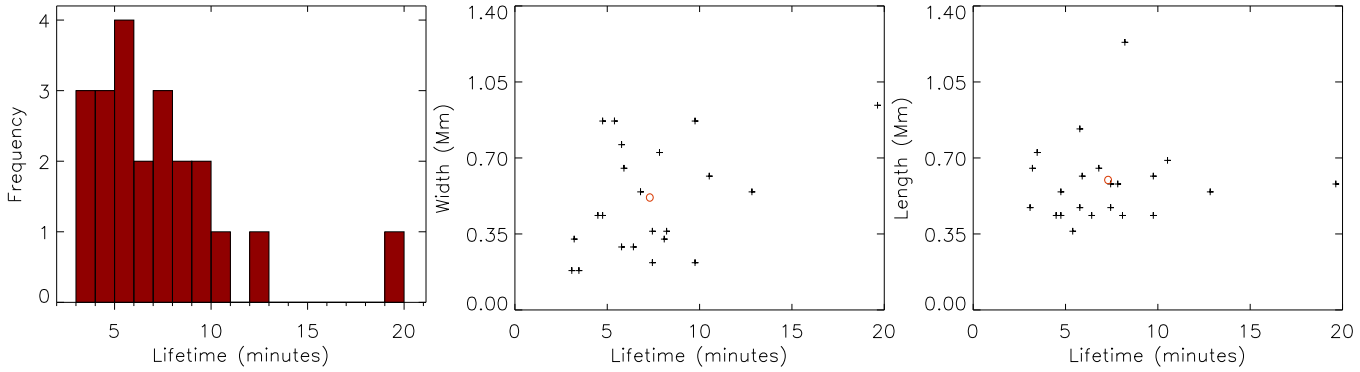


**Figure 3.** Basic statistical properties of EBs. Left: lifetime of each of the 22 identified events, with all but three events existing for less than 10 minutes. Center: distribution of peak width vs. lifetime. Right: same as center but for length. The red circles indicate the mean of both variables for each plot.

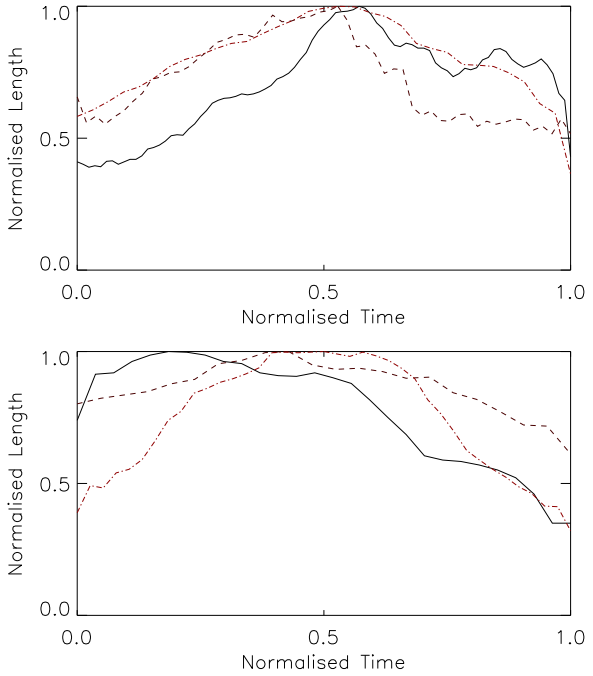


**Figure 4.** Smoothed projection profiles for the tips (normalized against the peak length of each event) of the three EB segments analyzed in Case Study: I (top) and three other independent EBs (bottom). Each event is plotted through its full lifetime. The top panel highlights the parabolic evolutions of each small segment, indicative of a repetitive driver. These profiles are similar to the majority of EB events, represented by the dashed and dot–dashed lines in the bottom panel.

the statistical properties (such as lifetime and area) of each EB event. It should be noted that parabolic and ballistic profiles would not be discernible within these data due to their similarity in the photosphere and the spatial resolution. Therefore, we use "parabolic" as an umbrella term for both profile types. Basic energy estimates of EBs (see, for example, Georgoulis et al. 2002) require both lifetime and area and, hence, it would appear that a correlation exists between lifetime and energy release. Future analysis with a larger statistical sample should further test this assertion.

In Figure 5, a representative EB event is plotted through its onset until it reaches its peak length. The EB appears simultaneously and co-spatially in both wings before extending away along a constant trajectory. The black lines in Figure 5 indicate the path of the EB over time. It is interesting to note that all but two of the EBs analyzed appear to have tips that extend and contract with parabolic profiles, however, horizontal motions within these events are also common. Each EB was carefully analyzed for both vertical and horizontal motions and the results were recorded. For the parabolic EBs identified, an average vertical speed of around 9 km $s^{-1}$ was observed (from onset to peak extension), with most events reaching higher velocities during their most explosive periods. It was found that 12 of the EB events analyzed here exhibited transverse motions, averaging at 1.5 km $s^{-1}$ (similar to velocities observed by, for example, Denker et al. 1995; Nindos & Zirin 1998); however, several EBs had apparent motions over 3 km $s^{-1}$. The average horizontal speed is slightly higher than previous estimates (by, e.g., Georgoulis et al. 2002; Watanabe et al.

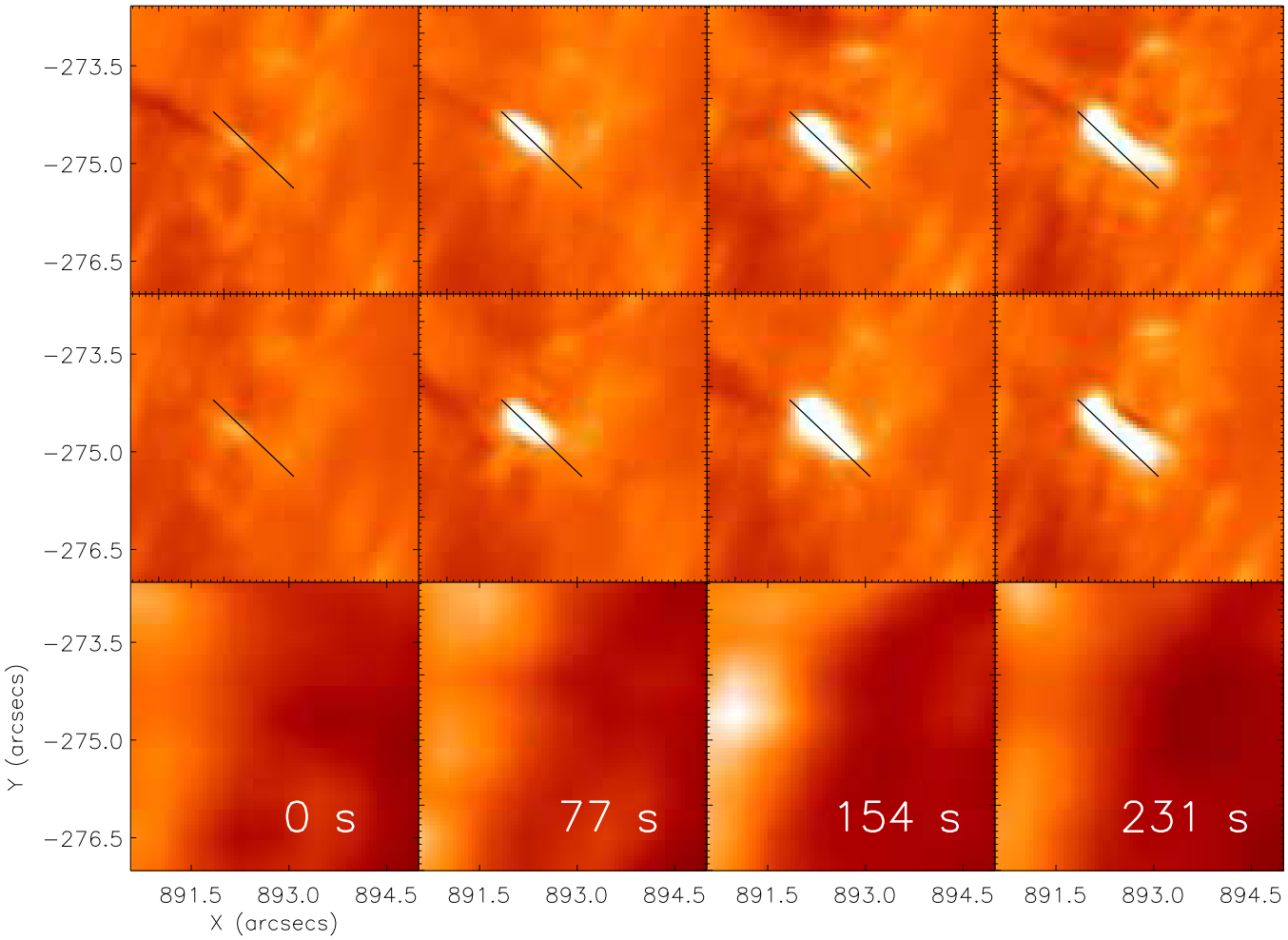


**Figure 5.** Evolution of EB event "A" (from Figure 1) in the blue (top) and red (middle) wings of the H$\alpha$ line profile with the co-spatial *SDO*/AIA 304 Å filter (bottom). The EB event appears in both wings simultaneously from an apparent footpoint before extending along a constant axis (identified by the black line of length 1200 km) to its peak length. After the fourth frame, it then fades back along the same axis. The initial images of this figure were taken at 17:32:30 UT and each subsequent image 77 s later.

2011; Nelson et al. 2013a), probably due to a small number of extremely dynamic events which are observed. We examine two EBs with significant horizontal speeds, and an apparent influence on the wider atmosphere, in detail in the following case studies.

Co-spatial EUV data inferred by the *SDO*/AIA instrument are also analyzed for each EB. As EBs consist of a vertical extension, one may expect that some signature would be observed in the upper atmosphere, however, the majority of previous studies have found no signal even within the H$\alpha$ line core (see, for example, Zachariadis et al. 1987; Watanabe et al. 2011; Vissers et al. 2013). Despite recent work by Bello González et al. (2013) suggesting that some EBs may penetrate into the chromosphere, it is still unclear whether these events have any influence on the chromosphere and corona. The EBs analyzed in this article show no influence in the upper atmosphere (although this lack of influence is to be expected within data collected at the limb), specifically within the H$\alpha$ line core, as indicated in Figure 1, or the EUV *SDO*/AIA filters, as plotted in Figures 5 and 6. Had co-spatial IRIS observations been available for this research, it would have been interesting to analyze what the overall influence of EBs is on the Transition Region plasma around 100,000 K.

As the intensity enhancement of an EB occurs in both wings of the H$\alpha$ line profile simultaneously and corresponds to apparent vertical motions, it is likely that these observables are a result of increased temperature and density within the ejected plasma compared to the surrounding atmosphere. This hypothesis agrees with simulations of EBs within the lower solar atmosphere (by, e.g., Fang et al. 2006; Nelson et al. 2013b), and with observations of flows co-spatial to EB events (e.g., Matsumoto et al. 2008). It has been widely speculated, as previously discussed, that magnetic reconnection in the photosphere could lead to plasma ejection, hence creating density increases in the local atmosphere similar to those observed here; however, it should be noted that no magnetic field data of sufficient resolution comparable to EB cross-sections are available for comparison to the CRISP data.

### *3.2. Case Study: I*

In these data, it is common that large, apparent horizontal motions are observed within EBs during their lifetimes. How these horizontal motions lead to interactions with plasma in the wider atmosphere is of specific interest and could prove key in assessing the potential influence of EBs within the

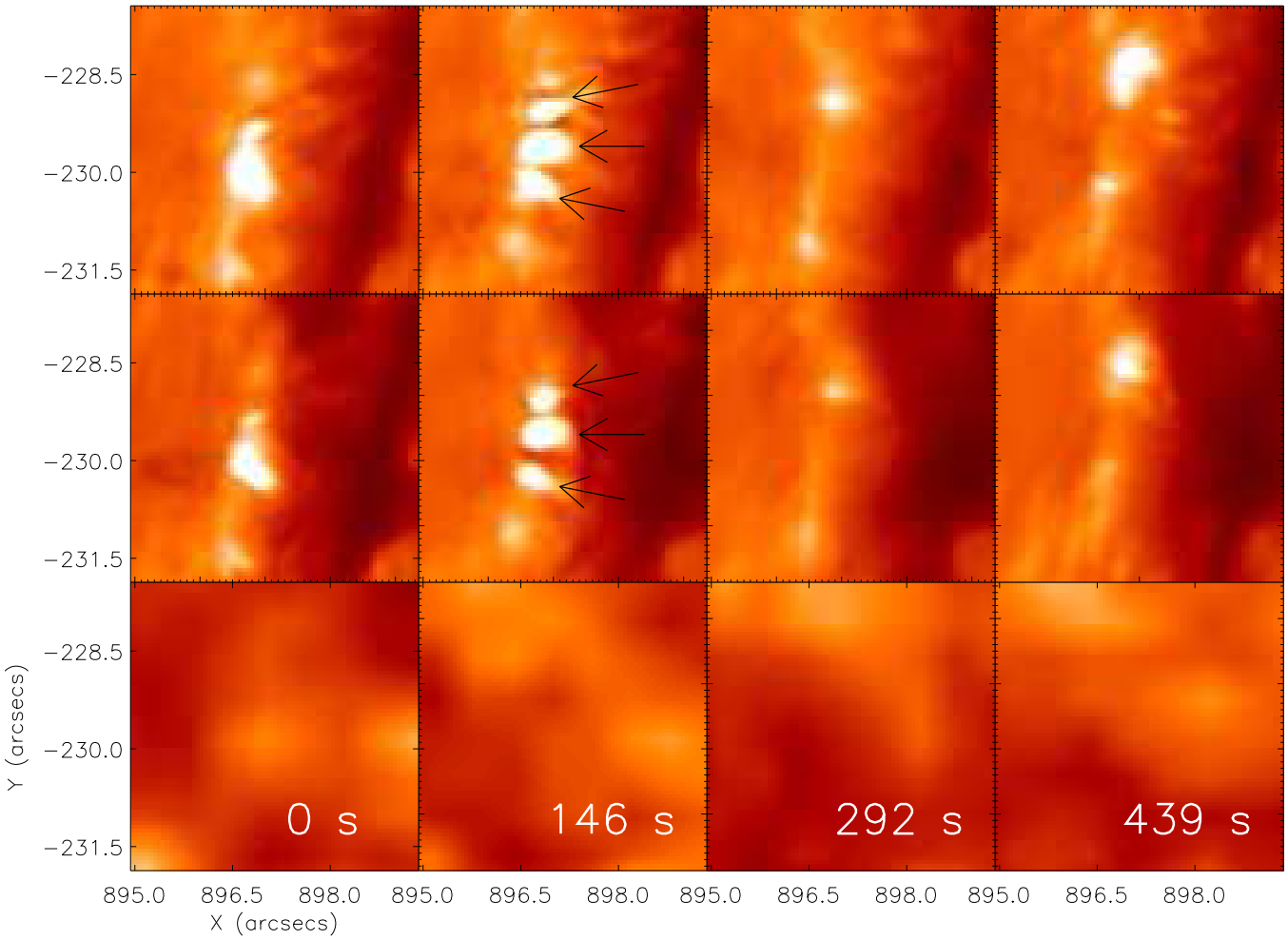


**Figure 6.** Illustration of the propagation of the EB analyzed in Case Study I for both the blue (−1 Å; top) and red (+1 Å; middle) wings of the H$\alpha$ line profile, as well as the *SDO*/AIA 304 Å filter (bottom). The almost northward propagation of this event appears to be parallel to the near-by penumbra and follows the bright track evident in the third panel. In the second panel for each wavelength, three small sub-structures are highlighted with arrows. The line wings are originally sampled at 7:29:54 UT and each subsequent image is separated by 146.3 s.

solar photosphere. In previous studies, it has proved difficult to accurately link EB events with any other solar phenomena and, hence, they have been analyzed as localized events. Here, we present one specific example of a region which appears to be susceptible to the formation of a number of EBs in a structured manner. EB events within this region display strong horizontal motions and appear to trigger other, similar events in different spatial locations.

In Figure 6, we plot the evolution of the northern event emphasized in Figure 1 with the label "CS1," with respect to time for both 6561.7 Å and 6563.83 Å (−1.1 Å and +1.03 Å from the line core, respectively). The first frame depicts the original EB, before spatial fracturing within this event is evident in the second frame (indicated by arrows). Each independent fracture appears to slowly propagate away from the original footpoint along the bright trail evident in the third frame. After the original EB fades for long enough such that it is deemed to have ended, a second large EB event occurs, as evidenced in the fourth frame. This rapid morphology is reminiscent of the evolution of the magnetic field simulated by, e.g., Archontis & Hood (2009), where an emerging flux rope formed in a "sea-serpent'-like manner reconnected at each individual ∪ to form a larger over-lying loop.

EBs have been shown to occur co-spatially with inter-granular lanes (see, for example, Denker et al. 1995; Nelson et al. 2013a). It is possible that the bright trail that appears to guide the EBs is evidence of a localized network structure, or an inter-granular lane. On-disk observations of the H$\alpha$ line wings often include weak intensity increases, reminiscent of this trail, co-spatial to strong magnetic fields, inferred using magnetogram or *G*-band data. It is, therefore, possible that these EBs are propagating along a defined structure and, hence, that further information could be derived by analyzing on-disk examples of such events. High-resolution, multi-wavelength observations close to the disk center should be further investigated to infer whether these events are indeed guided by the magnetic field.

It has been widely reported that EBs both migrate (for example, Denker et al. 1995; Nindos & Zirin 1998) and appear to recur, but what has not been presented yet in such detail, is a direct link between two apparently different, and highly structured, events. This does pose several important questions that can be discussed here. For example, what process is leading to the creation of multiple vertical peaks within this individual EB? If magnetic reconnection is indeed the driver of EBs, then, are we observing a "train" of reconnection through a "sea-serpentine" morphology as simulated by

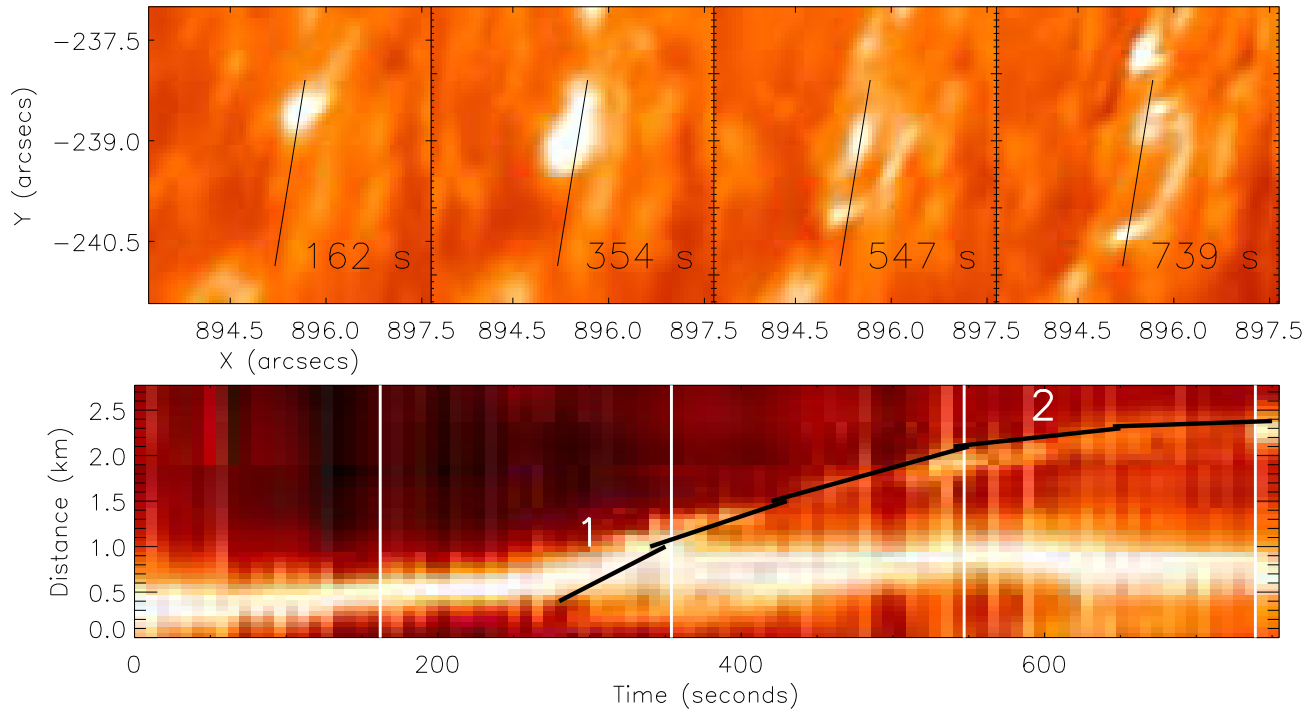


**Figure 7.** Evolution of the EB analyzed in Case Study II at +0.8 Å. In the top row, four frames from this wavelength are plotted starting at 7:40:49 UT and separated by 146.3 s. The initial EB event is easily observed in the left-hand frame. The most dynamic horizontal motion of the event is shown in the second frame before the generation of the apparent loop is depicted in the third and fourth frames. The bottom row shows the time-distance analysis of the black slit overlaid on the top row with intensity normalized through time to remove the influence of changes in seeing. The black line indicates the speed of the event through time, highlighting the evident deceleration. The speeds of the event at the times marked by 1 and 2 are 6.2 km s$^{-1}$ and 0.6 km s$^{-1}$, respectively. The white vertical lines depict the temporal position of each of the four top row plots.

Archontis & Hood (2009)? Thus, are sequential and apparently connected EBs a signature of a yet un-determined large-scale sub-surface process? The spatial separation between the initial and final EB event is around 2200 km, hence, this would suggest that a single reconnection event in a unstable region could lead to a sustained energy release within the local plasma (of course, this statement also applies if another driver is the cause of these events). For a full analysis of events such as this to be completed, high-resolution magnetic field data would be required, well beyond the current capabilities of instrumentation. It is, therefore, imperative that further research be carried out using both imaging observations and state-of-the-art computational modeling.

The second important result which can be drawn from this event is that small-scale EB dynamics, as discussed by Nelson et al. (2013a), are conspicuous within these data. It is inherently clear that higher-resolution data may allow further insight into the dependence, or indeed independence, of these small-scale events to close-by larger EB events. The individual parabolic profiles evident in each of the smaller-scale structures (Figure 4 (top)) analyzed in this example (analogous to the profiles observed in Figure 5) add weight to the argument that each fragment may be formed by a separate (or a single repetitive migrating) driver. Overall, we suggest that future analysis of EBs in a wide range of data sets be conducted to assess whether a minimum EB size is determinable using modern instrumentation.

### 3.3. Case Study: II

The final case study included within this article focuses on the event highlighted in Figure 1 by the box labeled "CS2." A number of interesting morphological features are observed during the evolution of this event which further evidence the dynamical nature of EBs. This EB exhibits the most rapid apparent horizontal motions observed in this data set (around 6 km s$^{-1}$), which occur during an apparent splitting of the event. Such dynamics have yet to be studied in the literature and provide a potentially excellent diagnostic tool for future analysis of the driver of EBs.

The evolution of the event is depicted by the top row of Figure 7, which shows information observed at +0.8 Å. The original EB, initial splitting, fading, and then loop formation are visualized from left to right, respectively. The bottom row of Figure 7 includes a time-distance plot for the spatial positioning indicated by the black line in the top row. The initial off-shoot appears to be as bright as the original EB event and propagates away from the formation site at a speed of 6.2 km s$^{-1}$. This is over four times the average apparent horizontal motion speed of EBs within these data. The off-shoot continues to move away from the large EB and decelerates until it reaches a speed of around 0.6 km s$^{-1}$. A black line is overlaid on the time-distance plot to emphasize the path of the off-shoot.

Of particular interest here is the similarity of this evolution to magnetic flux emergence events. Comparable morphological traits to these were reported by both Otsuji et al. (2007) and Ortiz et al. (2014). These researches analyzed events that had initial separation speeds of around 5 km s$^{-1}$ that dropped to around 1 km s$^{-1}$, and spatial separations of the footpoints on the order of 2200 km–3000 km. Flux emergence models also commonly discuss the occurrence of bright regions at the footpoints of formed loops (by such authors as Guglielmino et al. 2008), as observed here in the form of EBs. These brightenings have been

linked to reconnection between the emerging and existing fields and could facilitate the transport of energy from the lower solar atmosphere into the corona (as found to be, for example, by Isobe et al. 2008). Unfortunately, as this event occurs during the final frames of this data set, we are unable to establish whether this brightening and loop structure displays the traits observed in previous studies. Interestingly, Zachariadis et al. (1987) observed the occurrence of EB pairs, separated by around 3″. It is plausible that such pairs were formed in a comparable method to that described in this subsection.

In terms of EBs, this apparent link to an observation of flux emergence could prove exciting. Magnetic flux emergence has long been discussed as a potential driver of magnetic reconnection (see, for example, Heyvaerts et al. 1977; Shibata et al. 1992; Guglielmino et al. 2008) and, in particular, as a driver for EBs (suggested by, e.g., Georgoulis et al. 2002; Archontis & Hood 2009). We acknowledge that no co-spatial magnetic field data is available and, as such, we are unable to conclusively link this event with flux emergence, however, the similarities presented here are compelling. It should be noted by the reader that other alternatives exist to the flux emergence scenario, such as mass loading of an already existing loop. A larger-scale study of such events would be required to definitely answer this point. It is also unfortunate that these observations end co-temporally with the fourth frame of Figure 7, meaning that we are unable to analyze the full extent of this event. A variety of data sets should be analyzed in the near future to further test these findings, specifically in terms of how many EBs are actually linked to examples of flux emergence.

## 4. DISCUSSION

The results presented here support the conclusions of earlier investigations, where it has been suggested that EBs are energetic explosive events emanating from the lower solar atmosphere (see, for example, Georgoulis et al. 2002; Watanabe et al. 2011; Nelson et al. 2013b). The average lifetime and spatial properties of brightenings analyzed in this article (7 minutes and widths around 0.″65) are comparable to values reported by a number of authors as properties of EBs, therefore, allowing us to confidently link these near-limb events to on-disk EBs. However, we present the first limb measurements of EB lengths using state-of-the-art ground based instrumentation, finding the average height of these events to be 600 km (which is well below the believed height of formation for the H$\alpha$ line core of 2000 km). This is slightly shorter than previous estimates by Kurokawa et al. (1982). It should be noted that a plethora of highly dynamic events within our data were observed that did not eventually reach the required intensity threshold, possibly due to a mixing of events within the line-of-sight manifesting in a single less intense line profile. Because of this, we suggest that further study of EBs at the limb with a range of data sets could provide interesting additional insights.

We also find strong evidence of flows associated with EBs, agreeing with previous observations by, for example, Roy & Leparskas (1973) at the limb and Matsumoto et al. (2008) on the disk. The tips of 20 out of 22 events appear to follow a parabolic path through time suggesting the occurrence of a displacement of plasma, increasing the density and temperature within a localized region, hence, leading to the enhancement of the intensity in the wings of the H$\alpha$ line profile. We suggest that this propagation of plasma is analogous to the flows observed by Nelson et al. (2013b) at a simulated reconnection site where rapid cancellation of opposite polarity field occurred. Unfortunately, due to the FOV of these observations being situated at the solar limb, we are unable to confidently present co-temporal, co-aligned magnetic field data to analyze with this data set; hence, further assertions about the formation of these events elude us. We note, however, that no evidence of EBs within the H$\alpha$ line core or the *SDO*/AIA EUV filters is found, agreeing with previous studies, which have concluded that the vertical extensions of these events may not be sufficient enough to penetrate into the chromosphere and lower corona.

The two individual case studies presented in Section 3 highlight small-scale dynamics associated with EBs that have not previously been observed. Within the first case study, the influence of an EB on the surrounding atmosphere was analyzed. A large EB event appeared (by visual inspection) to fragment, with the small-scale pieces appearing to propagate north, away from the initial event. Each of the small-scale fragments were only around 230 km in diameter, similar in size to the events analyzed by Nelson et al. (2013a). The northern-most fragment drifted to around 1500 km from the initial position before reducing dramatically in size and fading below the threshold of 1.5 times the background intensity. A second large EB event was, then, observed to occur at the same spatial position. This case study highlights the influence that EBs can have on the surrounding localized plasma. Other examples of the horizontal extensions of EBs are also observed within these data, however, as these events are further toward the limb, we are unable to fully resolve any potential smaller-scale structures within the larger event.

The second case study discussed a rapid splitting of a large EB event close to a large sunspot. The main body of the ejection appeared to propagate south, away from the initial event, and continued through until the end of these observations, decelerating from around 6.2 km s$^{-1}$ to approximately 0.6 km s$^{-1}$. Possibly, the most interesting aspect of this example is the apparent loop formation between the two main bodies in the H$\alpha$ line wings, potentially indicating a flux emergence region (see, for example, Otsuji et al. 2007; Ortiz et al. 2014). Despite a significant apparent vertical extension of this loop, no evidence of any such structure within the H$\alpha$ line core was found (possibly due to the dense foreground structures in the H$\alpha$ line core obscuring any signal) suggesting that even a dynamic event, such as this example, has no initial influence on the upper chromosphere. Unfortunately, our observations end before the loop faded and we are unable to discuss the full evolution of this event. We strongly encourage that further work be carried out to fully test whether other flux emergence regions can be correlated to EBs.

Overall, we suggest that this analysis highlights both the small-scale structuring and dynamic nature of EBs. An investigation of a wide variety of these events at a range of spatial positions over the Sun would be required to fully understand how many EBs display morphologies similar to those discussed within the presented case studies. We have now addressed the importance of investigating the sub-structures of small-scale, explosive phenomena in the lower solar atmosphere that can act as important agents in triggering local instabilities in the magnetic environment of the solar surface. Such influence can be both vertically and horizontally orientated and require extensive future study.

Research at the Armagh Observatory is grant-aided by the N. Ireland Dept. of Culture, Arts and Leisure. We thank the UK Science and Technology Facilities Council for C.J.N.'s

and N.F.'s studentships, PATT T&S support, plus support from grant ST/J001082/1. The Swedish 1 m Solar Telescope is operated on the island of La Palma by the Institute for Solar Physics of Stockholm University in the Spanish Observatorio del Roque de los Muchachos of the Instituto de Astrofsica de Canarias. We thank L. Rouppe van der Voort (Institute of Theoretical Astrophysics, University of Oslo) for advice on data reductions with MOMFBD for SST/CRISP. R.E. is thankful to the NSF, Hungary (OTKA, Ref. No. K83133) and acknowledges M. Kéray for patient encouragement.

## REFERENCES

Archontis, V., & Hood, A. W. 2009, A&A, 508, 1469
Bello González, N., Danilovic, S., & Kneer, F. 2013, A&A, 557, A102
Cavallini, F. 2006, SoPh, 236, 415
de la Cruz Rodríguez, J., Löfdahl, M. G., Sütterlin, P., Hillberg, T., & Rouppe van der Voort, L. 2014, A&A (arXiv:1406.0202)
Demoulin, P., Henoux, J. C., Mandrini, C. H., & Priest, E. R. 1997, SoPh, 174, 73
Denker, C., de Boer, C. R., Volkmer, R., & Kneer, F. 1995, A&A, 296, 567
Ellerman, F. 1917, ApJ, 46, 298
Fang, C., Tang, Y. H., Xu, Z., Ding, M. D., & Chen, P. F. 2006, ApJ, 643, 1325
Georgoulis, M. K., Rust, D. M., Bernasconi, P. N., & Schmieder, B. 2002, ApJ, 575, 506
Guglielmino, S. L., Zuccarello, F., Romano, P., & Bellot Rubio, L. R. 2008, ApJL, 688, L111
Henriques, V. M. J. 2012, A&A, 548, A114
Heyvaerts, J., Priest, E., & Rust, D. M. 1977, SoPh, 53, 255
Isobe, H., Proctor, M. R. E., & Weiss, N. O. 2008, ApJL, 679, L57
Isobe, H., Tripathi, D., & Archontis, V. 2007, ApJL, 657, L53
Kurokawa, H., Kawaguchi, I., Funakoshi, Y., & Nakai, Y. 1982, SoPh, 79, 77
Lemen, J. R., Title, A. M., Akin, D. J., et al. 2012, SoPh, 275, 17
Matsumoto, T., Kitai, R., Shibata, K., et al. 2008, PASJ, 60, 95
Murphy, G. A., Rust, D. M., Strohbehn, K., et al. 1996, Proc. SPIE, 2804, 141
Nelson, C. J., Doyle, J. G., Erdélyi, R., et al. 2013a, SoPh, 283, 307
Nelson, C. J., Shelyag, S., Mathioudakis, M., et al. 2013b, ApJ, 779, 125
Nindos, A., & Zirin, H. 1998, SoPh, 182, 381
Ortiz, A., Bellot Rubio, L., Hansteen, V., de la Cruz Rodriguez, J., & Rouppe van der Voort, L. 2014, ApJ, 781, 126
Otsuji, K., Shibata, K., Kitai, R., et al. 2007, PASJ, 59, 649
Pariat, E., Aulanier, G., Schmieder, B., et al. 2004, ApJ, 614, 1099
Pariat, E., Schmieder, B., Berlicki, A., et al. 2007, A&A, 473, 279
Qiu, J., Ding, M. D., Wang, H., Denker, C., & Goode, P. R. 2000, ApJL, 544, L157
Roy, J.-R., & Leparskas, H. 1973, SoPh, 30, 449
Rutten, R. J., Vissers, G. J. M., Rouppe van der Voort, L. H. M., Sütterlin, P., & Vitas, N. 2013, JPhCS, 440, 012007
Scharmer, G. B. 2006, A&A, 447, 1111
Scharmer, G. B., Bjelksjö, K., Korhonen, T. K., Lindberg, B., & Petterson, B. 2003, Proc. SPIE, 4853, 341
Scharmer, G. B., Narayan, G., Hillberg, T., et al. 2008, ApJL, 689, L69
Sekse, D. H., Rouppe van der Voort, L., & De Pontieu, B. 2012, ApJ, 752, 108
Shelyag, S., Schüssler, M., Solanki, S. K., & Vögler, A. 2007, A&A, 469, 731
Shibata, K., Nozawa, S., & Matsumoto, R. 1992, PASJ, 44, 265
van Noort, M., Rouppe van der Voort, L., & Löfdahl, M. G. 2005, SoPh, 228, 191
Vissers, G., & Rouppe van der Voort, L. 2012, ApJ, 750, 22
Vissers, G. J. M., Rouppe van der Voort, L. H. M., & Rutten, R. J. 2013, ApJ, 774, 32
Watanabe, H., Vissers, G., Kitai, R., Rouppe Van Der Voort, L., & Rutten, R. J. 2011, ApJ, 736, 71
Zachariadis, T. G., Alissandrakis, C. E., & Banos, G. 1987, SoPh, 108, 227